JOURNAL OF MATERIALS SCIENCE 23 (1988) 3263–3271

Addition of $Ba_2TiSi_2O_8$ to manganese-doped barium titanate: effect on oxygen diffusion and grain-boundary composition

J. WEISS,* G. ROSENSTEIN
Philips Forschungslabor, Aachen, West Germany

The effect of barium titanium silicate additions to pure and manganese-doped barium titanate was studied by high-temperature conductivity and analytical electron microscopy. The results show that this addition precipitates during cooling as a second crystalline phase with only a small amount of amorphous phase left in a few grain boundaries. The secondary crystalline phase incorporates excess manganese left from the heterogeneous doping of barium titanate.

1. Introduction

The use of nickel electrodes in ceramic multilayer capacitors based on barium titanate requires that they are sintered under a reducing atmosphere. This necessitates the use of acceptor dopants in order to maintain the insulating state of the $BaTiO_3$ dielectric according to the defect chemistry [1–4]. The use of manganese as an acceptor has been described in a number of papers [2, 4–7]. A smooth temperature dependence of the relative permittivity, ε_r, requires a heterogeneous distribution of the dopant [8, 9].

On the other hand, manganese accumulations in the grain boundaries formed by locally exceeding the solubility, should be avoided, because they are suspected to be of higher conductivity. Thus the solubility limit of manganese in $BaTiO_3$ has to be determined. Earlier investigations only used up to 2 mol % [2, 10] without showing a solubility limit, while another paper reports higher concentrations with partial transformation to hexagonal $BaTiO_3$ again without reporting a solubility limit [5].

In order to avoid such manganese accumulations, it seemed of advantage to add small amounts (< 3 wt %) of $Ba_2TiSi_2O_8$ (BTS) to the $BaTiO_3$ matrix. The use of such silicate additions has been described in three earlier works [11–14]. Here it should serve two purposes:

1. BTS should "buffer" excess amounts of manganese by incorporating it into a second phase of either amorphous or crystalline nature.

2. BTS should aid sintering in order to support the heterogeneity of the dopant distribution by lowering the sintering temperature.

The following experiments should solve these questions. First, the reactions and the thermodynamics of such mixtures are evaluated by reacting $Ba_2TiSi_2O_8$ with $BaMnO_3$ and $MnSiO_3$ with $BaTiO_3$. This should serve as a simulation of possible reactions in the grain boundaries. DTA investigations should exploit the effect of composition and atmosphere for the melting temperature. Second, the solubility of manganese in $BaTiO_3$ under equilibrium conditions, is determined by measuring the Curie Point, T_c, in $BaTiO_3$ ceramics with increasing amounts of manganese. Finally, the microstructure of such a $BaTiO_3$ matrix with BTS additions should be evaluated on a macroscopic scale by high-temperature four-point conductivity measurements. These can reveal a distinct rise in the slope of the $\ln S$–$1/T$ line due to the softening point of the amorphous phase, when a large fraction of the grain boundaries contains a thin amorphous second phase. In addition, such an amorphous phase alters the bulk diffusivity of oxygen. This can be tested by measuring the time response upon a change in pO_2. Both types of conductivity measurement are done with $BaTiO_3$ and with $BaTiO_3$ containing BTS for comparison. Such macroscopic measurements seemed necessary, because even when an amorphous grain-boundary phase is detectable by analytical electron microscopy (AEM), no safe statement can be made, whether it is distributed equally over all grain boundaries or not.

On a microscopic scale this question should be checked by AEM, using dark-field imaging and scanning transmission electron microscopy (STEM) mode in combination with energy dispersive X-ray analysis (EDAX) analysis.

2. Experimental procedure

2.1. Powder preparation

The reactions between $BaMnO_3$ and $Ba_2TiSi_2O_8$, as well as the solubility limit of manganese in $BaTiO_3$, were studied with powders prepared by mixed oxides, with 1 h mixing in agate jars, calcining (15 h, 1150° C, air), and milling for 2 h in agate jars under hexanol. The BTS-type compositions were prepared by mixing and spray-drying the appropriate amounts of oxides and carbonates. They were calcined at 1050 or 1100° C for 50 h in order to achieve thorough reaction. After roller milling for 1 h with ZrO_2 media, these powders were attritor milled for 2 h to obtain the smaller par-

Present address: Renker GmbH, Hausener, Weg. D-7800, Frieburg, West Germany.

0022–2461/88 $03.00 + .12

TABLE I Composition, raw materials and powder analysis data.

Composition	BET ($m^2 g^{-1}$)	d_{50} (μm)	AAS analysis (wt %)			
			Mn	Si	Zr	Ca
$Ba_2TiSi_2O_8$	15.8	–				
Ba_1Ca_1Ti $Si_2Mn_{0.05}O_{8.1}$ (= BCTSM)	2.2	–				
$Ba_{1.5}Ca_{0.5}TiSi_2O_8$ (= G5)	16.5	–	n.d. = below detectability			
$Ba_{102.5}Ti_{100.6}Mn_1O_x$	5.5	0.56	0.22	0.04	0.24	n.d.
$Ba_{103.75}Ti_{100.6}Mn_2O_x$ (P8.5)	9.8	0.35	0.45	0.04	0.48	n.d.
$Ba_{105}Ti_{100.6}Mn_3O_x$	7.1	0.51	0.72	0.05	0.29	n.d.

The $BaTiO_3$ materials listed in Tables III and IV were prepared from:
Tam HPB, high-purity $BaTiO_3$, Tam, Niagara Falls, USA
$Ba(Ac)_2$ Alfa Products
$Mn(Ac)_2 \cdot 4H_2O$ Alfa Products

The $BaTiO_3$ materials listed in Table II were prepared from:
$BaCO_3$ Merck
TiO_2 Kronos
$MnCO_3 \cdot xH_2O$ Merck, x was determined by treating in dry $N_2/5\%$ H_2 at 1350° C, measuring the weight loss.

The silicates were prepared from:
TiO_2 Unitane $BaCO_3$ Merck
SiO_2 Merck
$Ca(Ac)_2$ Alfa Products
$Mn(Ac)_2 \cdot 4H_2O$ Alfa Products

ticle size necessary to achieve a better dispersion of BTS in the grain boundaries. The dried powders were then pressed into bars or pellets and fired as for the materials described below.

The powders for the conductivity measurements and for the TEM/STEM-EDAX analyses were prepared from high-purity $BaTiO_3$ Tam HPB (TAM, Niagara Falls, New York, USA). The doping with manganese was achieved by dissolving the appropriate amounts of manganese acetate and barium acetate ($MnAc_2$ and $BaAc_2$), in distilled water and adding it to a slurry of $BaTiO_3$ (300 g $BaTiO_3$ in 2000 cm^3 H_2O). $BaAc_2$ served to maintain an A/B lattice site ratio in $BaTiO_3$ of between 1.01 and 1.005 in the final product in order to inhibit grain growth (taking into account the average 0.5 wt % ZrO_2 wear from attritor milling). This mixture was stirred for 5 min and then spray-dried. The $BaTiO_3$ powders were calcined at 1150° C for 2 h in air. The compositions and the powder analysis data are listed in Table I.

These powders were then roller milled for 1 h using 1000 cm^3 of 2 cm ZrO_2 media on 400 g powder in porcelain jars under H_2O to which 200 cm^3 0.1 N oxalic acid was added to inhibit formation of water-soluble $Ba(OH)_2$. Then the slurry and media were transferred to a plastic bottle and milled for 1 h on a vibration mill. The powder was dried and sifted before attritor milling. This was done using 120 g powder and 1200 g 3 mm ZrO_2 media for 90 min. Again 100 cm^3 0.1 N oxalic acid were added to inhibit $Ba(OH)_2$ formation. The $BaTiO_3$ powders were milled for 90 min. After drying and sifting, the powder was heat treated for 1 h at 550° C to decompose the oxalic acid.

2.2. Preparation and sintering of samples for conductivity and microstructure analysis

In order to obtain larger samples for conductivity measurements, foils were stacked, pressed and cut. Mixing of manganese-doped $BaTiO_3$ with BTS was usually done by preparing the slurry for foil casting by treating the slurry with the organic binder system consisting of a wetting agent, solvent, dispersion agent and plastisizer as described previously [15, 16]. Foil casting was done by the doctor blade process. The foils were sectioned and cut. For most of the present investigations, wafers were made by stacking up to 50 layers of tape, which were subsequently pressed to form monolithic bodies. Then the binder was burnt out by slowly heating (16 h ramp) in air to 355° C.

All samples were sintered in $MoSi_2$ heated pipe furnaces in $N_2/0.2\%$ H_2 saturated with water vapour

TABLE II Composition, firing conditions and phase analysis of silicates and samples for the detection of the manganese solubility. These materials were prepared by the mixed oxide method

Composition	Sintering conditions			T_c (° C)	Phase analysis X-ray diffr.
	T (° C)	t (h)	Atm.		
Tam HPB	1300	1	N_2 0.2% H_2	121	t
$Ba_{100}Ti_{101}Mn_{0.5}O_x$	1350	4	FMG	106	t
	1350	4	air	119	t
$Ba_{100}Ti_{101}Mn_1O_x$	1350	4	FMG	104	t
	1350	4	air	119	t
$Ba_{100}Ti_{101}Mn_2O_x$	1350	4	FMG	79	t
	1350	4	air	121	t
	1450	4	FMG	112	t + h
$Ba_{104}Ti_{101}Mn_2O_x$	1450	4	FMG	79	t + h
$Ba_{100}Ti_{101}Mn_3O_x$	1350	4	FMG	89	t
	1350	4	air	119	t
$Ba_{101}Ti_{100}Mn_3O_x$	1350	4	FMG	–	open porosity
	1450	4	FMG	92	t + h
	1350	4	air	122	t
$Ba_{104}Ti_{100}Mn_3O_x$	1450	4	FMG	79	t + h
$Ba_{100}Ti_{102}Mn_4O_x$	1350	4	FMG	74	t + h
	1350	4	air	123	t + h

FMG = $N_2/5\%$ H_2 moisted in H_2O at room temperature.
t = tetragonal (at room temperature) $BaTiO_3$.
h = hexagonal $BaTiO_3$ stabilized by manganese to room temperature.

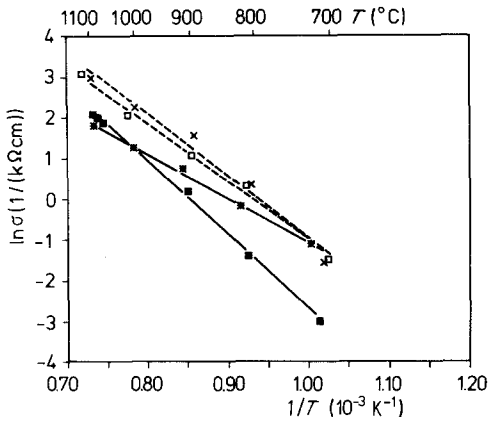

Figure 1 Temperature dependence of the electric conductivity measured by the four-point method in flowing O_2 in $BaTiO_3$ with and without BTS additions. (■) Tam HPB, (*) Tam HPB + 2 wt % BCTSM, (□) P8.5, (x) P8.5 + 2 wt % G5. Compositions and sintering conditions: see Table III.

at room temperature. The sintering conditions are listed in Table II.

2.3. Powder analysis

The powders prepared from Tam HPB as well as BTS-type powders were measured for specific surface area (BET). For several powders we also measured the particle size and size distribution by a Micromeritics sedigraph by dispersing them with an ultrasonicator for 5 min in H_2O, to which 0.5 wt % Na_2HPO_4 was added. The manganese content of several $BaTiO_3$ powders was analysed by atomic absorption spectroscopy (AAS). All these results are included in Table 1.

2.4. Analysis of phase composition and Curie temperature

Several specimens were analysed by X-ray diffraction for phase composition. These results are included in Table II. The solubility of manganese was checked by measuring the Curie point, T_c, of samples sintered at 1350° C or higher, for 4 h in N_2/5% H_2 also saturated by water vapour at room temperature. For comparison, identical compositions were sintered under otherwise identical conditions in air. The pellets were then vapour coated with NiCrAu to apply electrical contacts and measured on a Hewlett Packard bridge 4274 A from −60 to 150° C at 1 kHz, 1 V in order to determine the T_c value.

TABLE III Activation energy of the conductivity as determined from the Arrhenius plot of ln σ–$1/T$ by a least squares fit

Composition (sintered in moist N_2/0.2% H_2)	Sintering temperature (1 h) (° C)	Activation energy (eV)
Tam HPB	1260	1.6
Tam HPB + 1 wt % BCTSM	1260	1.1
Tam HPB + 2 wt % BCTSM	1260	0.6
Tam HPB + 4 wt % BCTSM	1260	0.8
Tam HPB + 8 wt % BCTSM	1260	1.0
$Ba_{102.5}Ti_{100.6}Mn_1O_x$	1350	1.1
$Ba_{103.75}Ti_{100.6}Mn_2O_x$ (P8.5)	1175	1.2
P8.5 + 1 wt % G5	1175	1.2
P8.5 + 2 wt % G5	1175	1.3
$Ba_{105}Ti_{100.6}Mn_3O_x$	1350	1.5
$Ba_2TiSi_2O_8$ (sint. in O_2)	1410	7.0

TABLE IV Diffusion constants estimated from the time response upon change in p_{O_2} from 1 to 0.1 bar (out) and from 0.1 to 1 bar (in). These values may be compared to D_0^{BT} = 5700 exp (−23780/T) (cm^2 sec^{-1}) from [16, 17]. The sintering conditions of the materials listed here are identical to those of Table III

Composition	Temperature (° C)	D_{out} (cm^2 sec^{-1})	D_{in} (cm^2 sec^{-1})
Tam HPB	810	6.9×10^{-5}	–
	905	1.5×10^{-4}	6.6×10^{-5}
	998	2.0×10^{-4}	4.2×10^{-4}
Tam HPB + 1 wt % BCTSM	815	6.6×10^{-5}	–
	908	1.5×10^{-4}	5.1×10^{-6}
	995	1.3×10^{-4}	1.7×10^{-4}
Tam HPB + 8 wt % BCTSM	815	4.5×10^{-5}	1.4×10^{-5}
	907	5.3×10^{-5}	1.0×10^{-5}
	995	6.3×10^{-5}	4.0×10^{-5}
$Ba_{102.5}Ti_{100.6}Mn_1O_x$	990	8.2×10^{-5}	2.4×10^{-5}
$Ba_{103.75}Ti_{100.6}Mn_2O_x$ (P8.5)	1018	2.5×10^{-4}	1.5×10^{-4}
P8.5 + 1 wt % G5	1001	8.3×10^{-5}	4.7×10^{-5}
P8.5 + 2 wt % G5	1002	6.2×10^{-5}	5.3×10^{-5}
$Ba_{105}Ti_{100.6}Mn_3O_x$	985	8.6×10^{-5}	–

2.5. Conductivity measurements

First, the high-temperature measurements of the electrical conductivity were performed in a canthal wound furnace in flowing oxygen. The oxygen partial pressure, p_{O_2}, was controlled by a ZrO_2 cell. The temperature was measured using an Ni/NiCr thermocouple stuck close to the sample. The conductivity was determined by the four-point method, for which the sintered dummy wafers were cut into bars of 2.0 cm × 0.5 cm and 0.2 cm thick. Notches to fix platinum contact wires were drilled alongside the bars at 0.1, 0.5, 1.5 and 1.9 cm on both sides. A detailed description of the experimental apparatus was given previously [17, 18]. In order to check for pure ohmic behaviour, the current was increased stepwise. The conductivity was calculated from the detected voltage by a least squares fit. All samples obeyed the ohmic behaviour well. The measured temperature range in O_2 at ambient pressure was 700 to 1100° C. This served to give the ln ϱ–$1/T$ diagram shown in Fig. 1, from which the activation energy was determined by a least squares fit. These results are listed in Table III.

Second, dynamic measurements were made by switching the gas flow between O_2 and N_2/10% O_2 following the change of conductivity over time. For this the gas flow of both gases was set at the same level (0.2 l min^{-1}). All samples were measured at 1000° C; some selected ones were additionally measured at 800 and 900° C. The percentage conductivity change over time then served to estimate the diffusion constant by a least squares fit of the function [19]

$$\ln (1 - C/C_0) = A + B t \qquad (1)$$

where C is the percentage change in voltage at time t, while C_0 is the change at infinity, for which in our case 5 to 10 min always proved to be sufficient. Using the sample thickness, h, the diffusion constant, D, at the temperature, T, can then be approximated by

$$D = (h^2/\pi^2)B \qquad (2)$$

The results are listed in Table IV.

2.6. Analytical electron microscopy investigations

For TEM/STEM microscopy the materials were cut by a diamond saw in to thin sections. These were then mechanically thinned to about 30 μm by mechanical grinding. Argon-ion milling was used to complete the thinning process. For the analytical investigations we used a Philips 400 T electron microscope, equipped with a scanning and energy dispersive analysis unit. The TEM mode was used for bright- and dark-field images. Dark-field images, with the objective diaphragm set on the amorphous ring of the corresponding diffraction pattern, were taken to reveal amorphous phases. STEM-EDAX digital linescans served to investigate the distribution of the elements silicon, manganese and calcium over particular areas. The STEM image with the marked location of the linescan shows relative characteristic X-ray intensities of these three elements along this scan. Each intensity was normalized by the sum of all measured intensities to reduce the influence of varying sample thickness, surface topography and primary electron intensity. Grain boundaries are drawn into these diagrams as vertical bars.

3. Results and discussion

3.1. Solubility of manganese in $BaTiO_3$ and reaction between excess manganese and BTS under various conditions

Fig. 2 shows the effect of manganese on T_c in $BaTiO_3$: while under reducing atmosphere, a linear decrease up to 2 mol % and 70° C is observed, oxidizing sintering alters this pattern such that hardly any change occurs. This is due to the absence of a significant concentration of oxygen vacancies, V_0^{BT}. The slope and the stable T_c upon sintering in air is found to be in agreement with results reported previously [4, 20]. Although from the thermodynamic point of view the solubility limit of manganese in $BaTiO_3$ may alter with p_{O_2}, such a change should be minimal compared to the absolute manganese content investigated here. Exceeding the solubility of manganese can lead to the formation of hexagonal $BaTiO_3$ in agreement with the results of Herbert [5]. Glaister and Kay [21] reported a lowering of the cubic to hexagonal conversion in $BaTiO_3$ in the presence of 10 mol % manganese down to 1100° C under reducing conditions. In the present investigation, the hexagonal $BaTiO_3$ modification could be identified as big needle-shaped crystals in the microstructure (Fig. 3) when sintered above 1300° C. The phase relation between the extreme compositions $BaTiO_3$ and $BaMnO_3$ is not reported in literature and was not a topic of the present investigation.

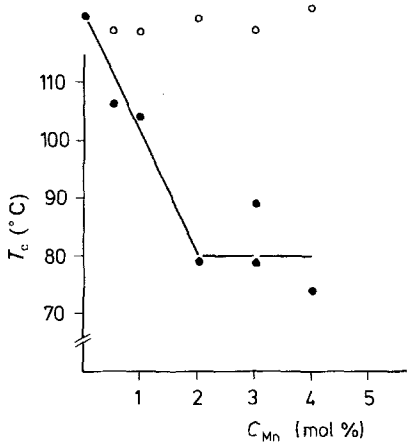

Figure 2 Solubility of manganese in $BaTiO_3$ sintered in (●) moist $N_2/5\%$ H_2 and (○) air. For A/B ratio and sintering conditions see Table II.

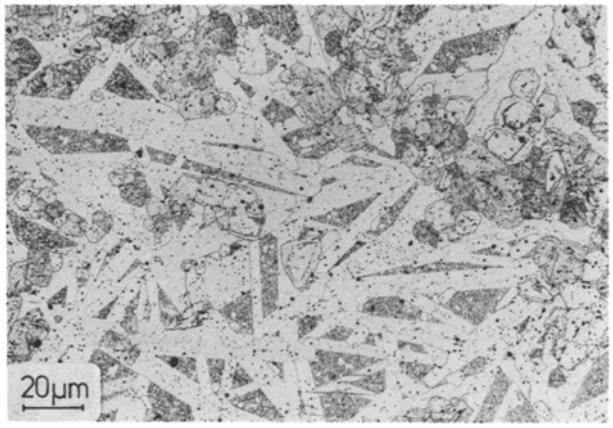

Figure 3 Stabilization of large needle-shaped hexagonal $BaTiO_3$ by manganese. Composition: $Ba_{104}Ti_{101}Mn_2O_x$, sintered at 1450° C, 4 h in moist $N_2/5\%$ H_2.

The X-ray diffraction analysis of mixtures of both $Ba_2TiSi_2O_8$ with $BaMnO_3$ and $BaTiO_3$ with $MnSiO_3$ gives the following reactions, when mixtures of these prereacted starting compounds are fired together.

$$Ba_2TiSi_2O_8 + BaMnO_3$$
$$\xrightarrow{O_2\ 1150°C} BaTiO_3 + Ba_2TiSi_2O_8 \text{ ss (Mn)}$$
$$\xrightarrow{O_2\ 1250°C} \text{melts}$$
$$\xrightarrow{FMG\ 1150°C} BaTiO_3 + Ba_2TiSi_2O_8 \text{ ss (Mn)}$$
$$\xrightarrow{FMG\ 1250°C} BaTiO_3 + Ba_2TiSi_2O_8 \text{ ss (Mn)} \quad (1)$$

$$BaTiO_3 + 2MnSiO_3$$
$$\xrightarrow{O_2\ 1150°C} \text{melts}$$
$$\xrightarrow{FMG\ 1150°C} Ba_2TiSi_2O_8 + MnTiO_3$$
$$\xrightarrow{FMG\ 1200°C} \text{melts} \quad (2)$$

FMG = $N_2/5\%$ H_2 saturated with water vapour at room temperature; ss = solid solution, see text. Only on the left-hand side is this reaction expressed quantitatively. On the right-hand side the complexity of the X-ray patterns and the fact that in all cases minor, unidentifiable peaks occurred, did not allow a quantitative evaluation. These unidentified phases will, however, not play a role for smaller amounts of BTS added to $BaTiO_3$. In such compositions they were never detected, but only $BaTiO_3$ and BTS were found.

Reaction 1 shows that under reducing conditions, excess manganese (forming $BaMnO_3$ in the extreme case) will be incorporated into BTS. A phase $Ba_2MnSi_2O_8$ is known from the literature [22]. Its X-ray pattern shows a striking similarity to that of BTS and does not allow a clear separation of these

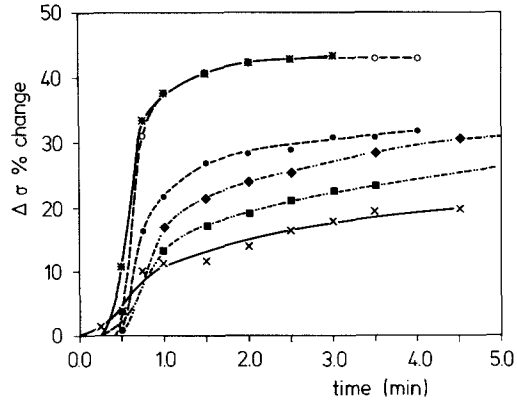

Figure 4 Time response of the change in conductivity upon switching the gas flow from O_2 to N_2/10% O_2. At 810° C: (○) Tam HPB, (×) Tam HPB + 1 wt % BCTSM, (■) Tam HPB + 8 wt % BCTSM. At 995° C: (●) Tam HPB, (*) Tam HPB + 1 wt % BCTSM, (◆) Tam HPB + 8 wt % BCTSM. For compositions and sintering conditions see Table III.

phases: the lattice parameters given [22] (a = 0.381 nm, c = 0.537 nm, tetragonal structure) differ little from those of $Ba_2TiSi_2O_8$ (a = 0.852 nm, c = 0.521 nm, tetragonal [23]). This case is indicated as BTS solid solution (Mn) in the reactions above. Although such a solid solution between these two related phases (exchanging manganese for titanium) was not investigated in detail, it does seem likely. The reason is the similarity of the structures and lattice constants [22–24]. In any case BTS does show some solubility for manganese as detected by STEM/EDAX measurements described below. Reaction 2 serves as a cross check for the opposite direction of Reaction 1, although of course its total composition is not identical to that of Reaction 1, which is the reason why $MnTiO_3$ is found in addition to BTS.

Replacement of part of the barium in BTS by calcium was checked by X-ray diffraction and always yielded BTS without any other phase. BTS itself does not change the solubility limit of manganese in $BaTiO_3$ in a visible manner. The T_c values of all materials were unchanged, when BTS was added.

DTA runs of mixtures of $BaTiO_3$ with BTS showed for manganese-free compositions a melting range of 1240 to 1300° C and for manganese-containing compositions 1180 to 1240° C. Calcium substituted in $Ba_2TiSi_2O_8$ for barium did not change the melting range in a detectable manner.

In these compositions, consisting of $BaTiO_3$ and BTS, variations of the p_{O_2} of the atmosphere (moist N_2 5% H_2 or air) did not show a different range of melting and phase composition. T_c and conductivity measurements of Tam HPB with addition of different amounts of a calcium, manganese containing BTS, revealed a partial acceptor doping from such a BTS during sintering. The doping content in $BaTiO_3$, of course, depends on the composition and amount of BTS added as well as on the sintering temperature.

3.2. Conductivity measurements

3.2.1. Some theoretical considerations

In $BaTiO_3$ at high temperatures (> 600° C) the conduction is of an electronic nature. Changes of the external p_{O_2} lead to a change in V_0^{BT}, so that dynamic measurements are controlled by the oxygen vacancy diffusion. For static measurements only the defect concentration plays a role. All this is well documented [1–4, 25, 26].

In an amorphous glassy phase, on the other hand, the conduction is governed by ionic diffusion, i.e. in silicate-rich glasses normally by the diffusion of oxygen ions or cations. So first of all the softening point of such a glass should change the slope of the

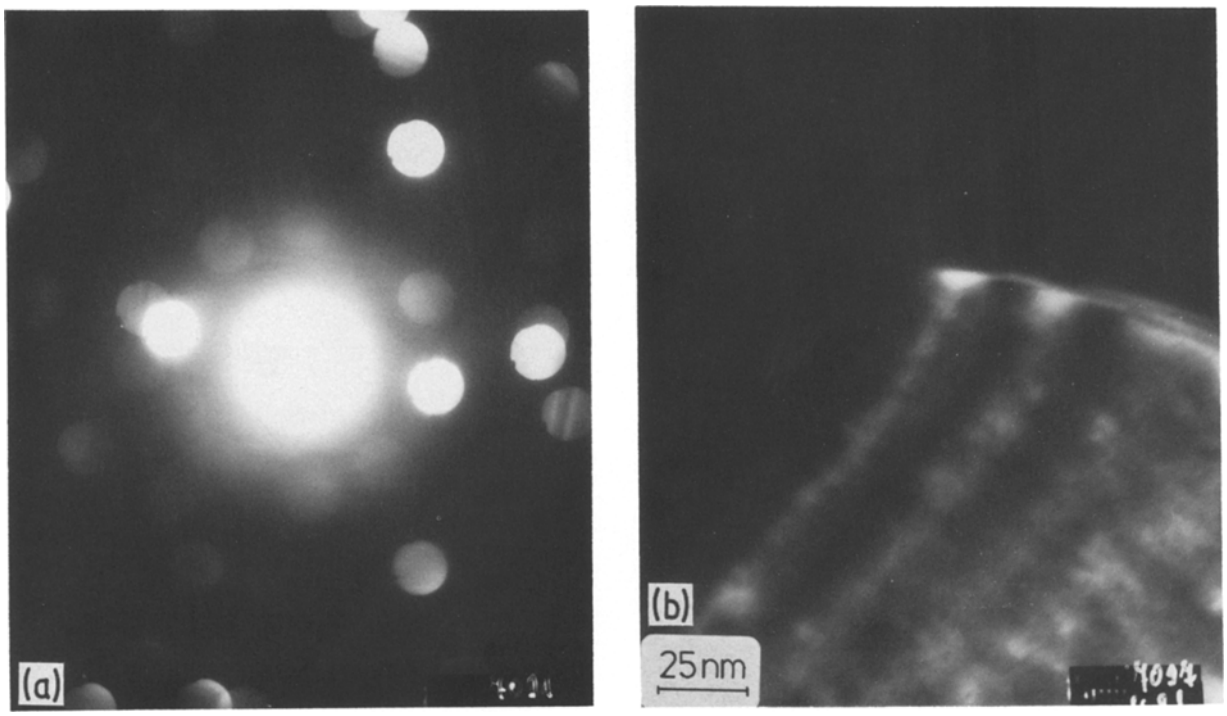

Figure 5 (a) Diffraction pattern (camera length L = 1600 mm) and (b) dark-field image taken by setting the objective aperture on the amorphous ring. Material: Tam HPB + 2 wt % BCTSM (for composition and firing see Table III). The dark-field image does not show any amorphous area.

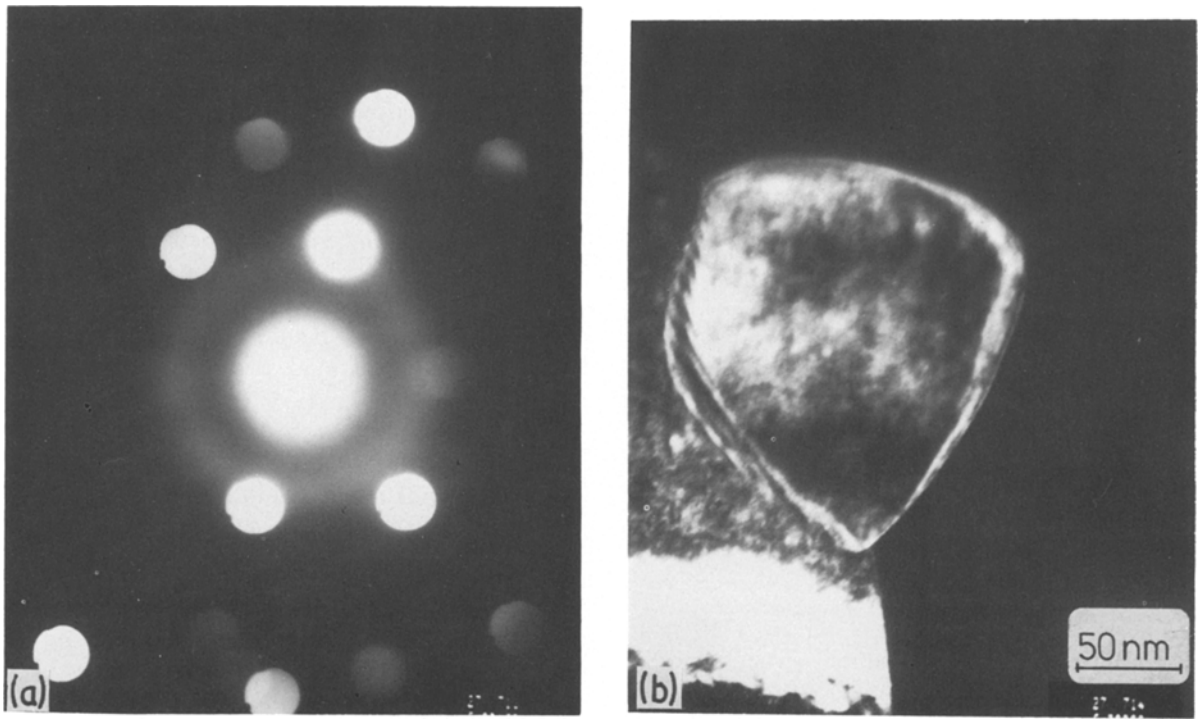

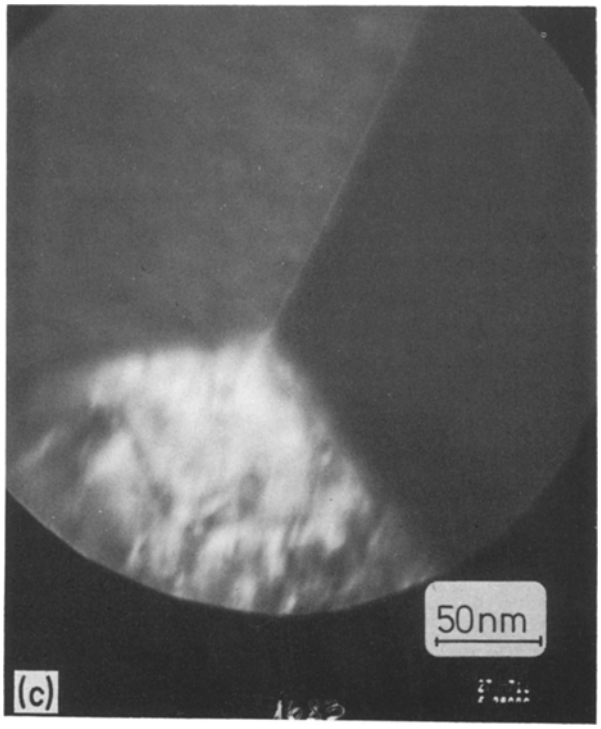

Figure 6 P8.5 + 1 wt % G5 (see Table III): (a) diffraction pattern (L = 1600 mm) and (b) dark-field image showing a grain surrounded by some amorphous phase. (c) One of the grain boundaries in a dark-field image with a thin amorphous layer.

conductivity, when plotted against the reciprocal temperature. Above a certain temperature the conductivity will no longer follow a simple Arrhenius-type behaviour due to other diffusion mechanisms that start to participate. Owing to the different activation energies, the temperature dependence of the conductivity should be different, when an amorphous grain-boundary phase is present and wets the grain boundaries.

Secondly, the presence of such an amorphous phase can alter the overall diffusion coefficient. The response time upon changes in p_{O_2} may vary considerably. For this overall diffusion coefficient the diffusivity of the amorphous phase is of importance. As it is strongly composition dependent (at 1000° C, D_O^{glass} ranging from 5×10^{-5} cm^2 sec^{-1} for 30% alkaline-containing silicate to 10^{-14} cm^2 sec^{-1} for pure SiO_2 glass [27]), only a rough estimate for the diffusion constant can be made. Thereby possible charge transport by cationic species (in the present case this would mainly be Ba^{2+}, because silicon, manganese and titanium as network formers are not likely to participate) can be neglected. As in these measurements the atmosphere was only varied between O_2 and N_2/10% O_2 and only the change in conductivity was detected (where the cations would give a constant contribution due to the small change in p_{O_2}), only oxygen diffusivity needs to be considered. The oxygen in glass can diffuse either as molecular oxygen or, as would be the case here, with the $BaTiO_3$ matrix, by network diffusion as ionic O^{2-} [28]. Taking into account these facts, the oxygen diffusion of such an amorphous phase will be several orders of magnitude lower than that in $BaTiO_3$ and thus should have a marked effect on overall diffusivity.

3.2.2. Temperature dependence of conductivity

The temperature dependence of the conductivity of $BaTiO_3$ and $BaTiO_3$–BTS mixtures in Fig. 1 shows a linear behaviour without any distinct bend. The addition of manganese to $BaTiO_3$ in BTS-free $BaTiO_3$ diminishes the activation energy at first and then increases it (Table III). This may be caused by exceeding the solubility limit of manganese in $BaTiO_3$ ($\sim$2 at. %, see Section 3.1). All activation energies, however, are within a range measured for diffusion in $BaTiO_3$ ceramics [17, 18]. It must be emphasized, that our values for the activation energies, as well as for the

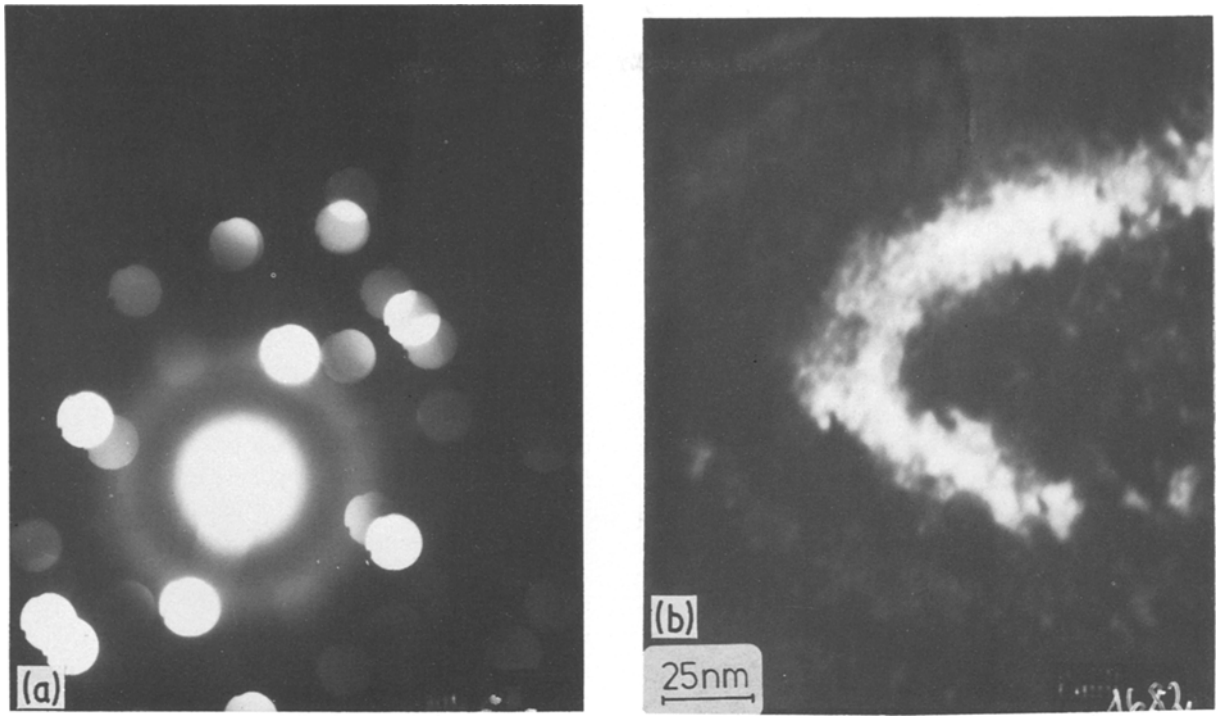

Figure 7 P8.5 (see Table III): (a) diffraction pattern (L = 1600 mm) and (b) dark-field image showing second phase microcrystals presumably embedded in amorphous phase. In this material the silica content is a result of wear by attritor milling.

diffusion constants, may not be considered as accurate material values themselves, due to the heterogeneous doping of the material, but serve to evaluate the microstructure. Expansion measurements of Tam HPB containing different levels of BTS carried out in air only revealed a very weak indication of a softening point at about 850° C, when the composition was very rich (about 30 mol %) in BTS. This also indicates the absence of significant amounts of an amorphous phase.

3.2.3. Diffusivity of oxygen upon changes in p_{O_2}

The time response of the change of the voltage upon change in p_{O_2} does not show any difference between silicate-containing and silicate-free material either. Fig. 4 shows two BTS-free and two BTS-containing materials for comparison. A percentage representation for the conductivity change was chosen to standardize the conductivities measured and make them comparable.

The diffusion coefficients estimated from these data are in the range of the diffusion coefficients determined for pure $BaTiO_3$ or slightly larger [17, 18]. This contradicts the presence of a continuous amorphous grain-boundary layer. The experimental evidence for the absence of an amorphous grain-boundary layer is also supported by the fact that both types of materials behave similarly at all three temperatures tested. This would require similar activation energies for the diffusion constants in both phases. Taking into account their different structure, this is unlikely. Assuming the detected crystalline nature of BTS, its amount is below the sensitivity level which would have any visible effect on the bulk diffusion in $BaTiO_3$.

3.3. TEM, STEM and EDAX analysis

Numerous papers describe the methods applicable for

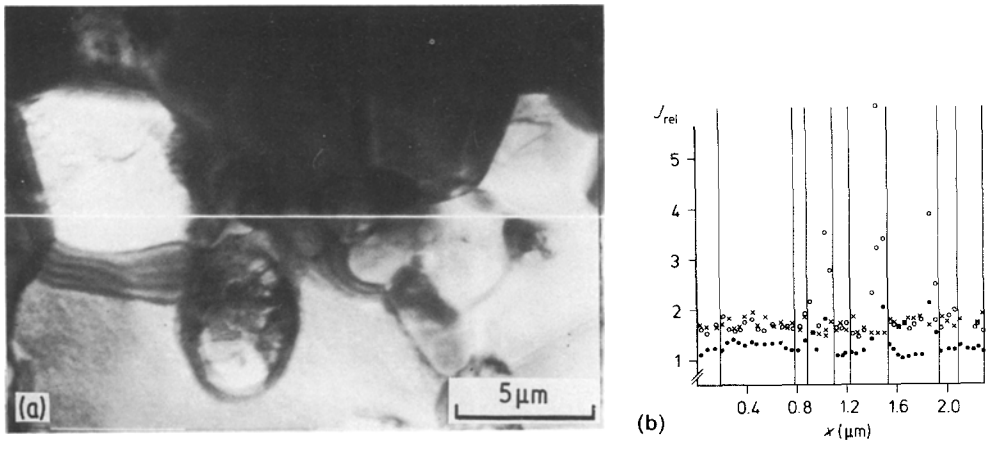

Figure 8 (a) STEM image and (b) EDAX line scan, revealing the accumulation of manganese and silicon in submicrometre-sized grains in the grain boundaries (material: P8.5 + 1 wt % G5) (b) (●) Si, (x) Ca, (○) Mn, V = 50 000, S = 10 nm.

the detection of thin amorphous grain-boundary layers in ceramic materials [29–31]. Because of the number of specimens to be investigated, dark-field images with the corresponding diffraction patterns were used to detect the presence or absence of an amorphous phase. Figs 5 to 7 show examples of this investigation, which again included BTS-free and BTS-containing material. The results are identical for both. In both types of material minimal amounts of amorphous phase can be found in a few grain boundaries. When such an amorphous layer is present in other types of materials like silicon nitride sintered with oxide additives, it would have a thickness of $\geqslant 2$ nm [30–32]. It was not possible in any case, to detect an amorphous grain-boundary layer as a continuous network on a large number of $BaTiO_3$ grains. The majority of the grain boundaries did not show any amorphous phase in the dark-field image, even when the grain boundaries were aligned exactly parallel to the electron beam. In addition, only in one case was it possible to detect a large number of very fine microcrystals in a triple point. From the diffraction pattern as well as the dark-field image, it appears that some amorphous phase may still be present between these microcrystals (Fig. 7). In no case did we observe large pools of amorphous phase in triple points. The fact that even in $BaTiO_3$, where no BTS was added, traces of an amorphous phase can be found, stems from the SiO_2 content, used as a sintering aid in the fabrication of the ZrO_2 attritor milling media (silicon content in the ZrO_2 media as detected by AAS; 4.61 wt %).

The STEM-EDAX line scan in Fig. 8 shows an enrichment of manganese and silicon in a small grain ($d \approx 0.2\,\mu$m) in a triple point between larger $BaTiO_3$ grains ($d \approx 1\,\mu$m). This supports the finding of the reaction study, that BTS reacts with the excess manganese in manganese-rich $BaTiO_3$ and incorporates it into its structure on titanium sites. Such microcrystals showing a high relative intensity of silicon and manganese have been detected in a number of locations. The calcium intensity had uniform distribution and did not show any enrichment in the silicate.

In order to estimate how much amorphous phase would be needed to form a uniform layer of 2 nm in all grain boundaries, we make the following estimation. The density of BTS, ϱ_{BTS} (4.45 g cm^{-3} [23]), may be approximated as 4.0 g cm^{-3} in the amorphous state. With the density, ϱ_{BT}, of $BaTiO_3$ taken to be 5.8 g cm^{-3}, the layer thickness $dx = 2$ nm of the amorphous phase, and the average grain size for $BaTiO_3$ 1 μm, the volume fraction, V_{gb}, of the amorphous phase is estimated according to the formula given by Saltikov [33]

$$V_{gb} = 2dx/d_g \quad (3)$$

which gives the weight fraction by using the densities

$$\text{wt}\,\%_{gb} = V_{gb}\varrho_{gb}100/(V_{gb}\varrho_{gb} + V_{BT}\varrho_{BT}) \quad (4)$$

This yields a value of 0.28 wt %. This theoretical estimation also shows that the amount BTS added should by far be sufficient to cover all grain boundaries. The fact that only a few grain boundaries and no triple points show such an amorphous phase is an indication that in $BaTiO_3$ a strong tendency exists to crystallize such a silicate second phase.

4. Conclusion

The solubility of manganese in $BaTiO_3$ and the effect of BTS additions to manganese-doped $BaTiO_3$ were the focal points of the present study. Thereby a particular point of interest was, whether, after cooling, BTS forms a crystalline second phase or remains present as an amorphous grain-boundary phase. The results show:

1. Manganese is soluble up to 2 mol % in $BaTiO_3$ under conditions that allow a homogeneous doping distribution. Heterogeneous doping normally will lead to local enrichment of manganese in grain boundaries already with lower levels of manganese content.

2. BTS aids densification by forming a liquid phase above 1240° C. The exact melting temperature is determined by the composition: whereas partial replacement of barium by calcium in $Ba_2TiSi_2O_8$ does not alter the melting point, manganese leads to a decrease of about 60° C.

3. BTS reacts with $BaMnO_3$, which may be present due to the high amount of manganese, exceeding the solubility limit of manganese in $BaTiO_3$ to form BTS ss, where manganese substitutes part of the titanium in $Ba_2TiSi_2O_8$. This is found by a direct reaction study as well as by STEM-EDAX analysis of manganese-rich $BaTiO_3$, to which BTS is added.

4. TEM diffraction and dark-field analysis yields only traces of an amorphous phase in a few grain boundaries. The presence of an overall amorphous grain-boundary layer may be ruled out, because BTS crystallizes after cooling.

5. High-temperature conductivity measurements in O_2 support this finding on a macroscopic scale. In addition, the conductivity does not show a bend when plotted against the reciprocal temperature, which otherwise should occur due to the softening point. Secondly, the time dependence upon changes in p_{O_2} does not show any effect when BTS is present.

Acknowledgements

The authors thank Dr H. Passing for carrying out the reaction study, J. Markowicz for the AAS analysis, H. D. Bausen for the X-ray diffraction study, and Drs J. Akse, D. Hennings and R. Waser for helpful discussions and advice.

References

1. J. DANIELS, *Philips Res. Rept.* **31** (1976) 505.
2. H. J. HAGEMANN and H. IHRIG, *Phys. Rev. B* **20** (1979) 3871.
3. N. H. CHAN, R. K. SHARMA and D. M. SMYTH, *J. Amer. Ceram. Soc.* **65** (1982) 167.
4. N. G. EROR and U. BALACHANDRAN, *ibid.* **65** (1982) 426.
5. J. M. HERBERT, *Trans. Brit. Ceram. Soc.* **62** (1963) 645.
6. I. BURN and G. H. MAHER, *J. Mater. Sci.* **10** (1975) 633.
7. I. BURN, *ibid.* **14** (1979) 2453.
8. M. S. H. CHU, T. C. DEAN and Ch. E. HODGKINS, "High K (4000) X7R composition for multilayer ceramic capacitors", paper presented at the 87th annual meeting of the

American Ceramic Society, 5–9 May 1985, Cincinatti (see *Bull. Amer. Ceram. Soc.* **64** (1985) 462 for abstract).
9. D. HENNINGS and G. ROSENSTEIN, *J. Amer. Ceram. Soc.* **67** (1984) 249.
10. H. IHRIG, *J. Phys. C. Solid State Phys.* **11** (1978) 819.
11. A. INZENHOFER, *Sprechsaal* **111** (1978) 567.
12. J. P. GUHA and D. KOLAR, "Phase equilibria, sintering characteristics and dielectric properties in the $BaTiO_3$ rich portion of the system $BaO–TiO_2–SiO_2$", Paper at a Conference on Electronic Ceramics, 8–15 May 1974, Kvalore, CSSR.
13. N. KÖPPEN and A. DIETZEL, *Glastechn. Ber.* **49** (1976) 199.
14. G. KOSCHEK and E. KUBALEK, *Beitr. elektronenmikroskop. Direktabb. Oberfl.* **16** (1983) 19.
15. I. BURN, *Bull. Amer. Ceram. Soc.* **50** (1971) 501.
16. V. F. CAPOZZI, "Multilayer ceramic capacitor materials and manufacture" (Oxy. Metal. Ind. Corp., Nutley, New Jersey, 1975).
17. R. WERNICKE, PhD thesis, RWTH Aachen, West Germany (1975).
18. *Idem, Philips Res. Rep.* **31** (1976) 526.
19. W. JOST and K. HAUFFE, "Diffusion, Methoden der Messung und Auswertung", 2nd Edn (Steinkopff, Darmstadt, 1972).
20. H. J. HAGEMANN, PhD thesis, RWTH Aachen, West Germany (1980).
21. R. M. GLAISTER and H. F. KAY, *Proc. Phys. Soc.* **76** (1960) 763.
22. N. di CESARE BRISI and F. ABBATTISTA, *Atti Accad. Sci. Torino* **95** (1960–61) 263.
23. S. HAUSSÜHL, J. ECKSTEIN, K. RECKER and F. WALLRAFEN, *J. Cryst. Growth* **40** (1977) 200.
24. A. HALLIYAL, A. S. BHALLA, S. A. MARKGRAF, L. E. CROSS and R. E. NEWNHAM, *Ferroelect.* **62** (1985) 27.
25. P. GERTHSEN, K. H. HÄRDTL and A. CSILLAG, *Phys. Status Solidi A* **13** (1972) 127.
26. J. MAIER, G. SCHWITZGEBEL and H. J. HAGEMANN, *J. Solid State Chem.* **58** (1985) 1.
27. J. SCHLICHTING, *High Temp. High Press.* **14** (1982) 717.
28. W. D. KINGERY, H. K. BOWEN and D. R. UHLMANN, in "Introduction to Ceramics", 2nd Edn (Wiley, New York, 1976).
29. G. THOMAS, D. R. CLARKE and O. van der BIEST, "The impact of transmission electron microscopy in ceramics", in "Ceramic Microstructures", edited by R. M. Fulrath and J. A. Pask, (Westview, Boulder, Colorado, 1977) pp. 29–53.
30. G. THOMAS and M. J. GORINGE, "Transmission Electron Microscopy of Materials" (Wiley, New York, 1979).
31. D. R. CLARKE, *Ultramicroscopy* **4** (1979) 33.
32. P. GREIL and J. WEISS, *J. Mater. Sci.* **17** (1982) 1571.
33. S. A. SALTIKOV, "A stereological method for measuring the specific surface area of metallic powders", (Springer, Berlin, 1967) pp. 63.

Received 17 September 1987
and accepted 11 January 1988